Sea Ice Motion, Age and Thickness from Synthetic Aperture Radar Imagery

Ron Kwok[1], Glenn F. Cunningham[1], Nettie LaBelle-Hamer[2],
Benjamin Holt[1] and Drew Rothrock[3]
[1]*Jet Propulsion Laboratory, California Institute of Technology*
[2]*Alaska SAR Facility, University of Alaska*
[3]*Polar Science Center, University of Washington*

Synthetic Aperture Radar (SAR) provides an amazingly detailed look at sea ice, but the level of detail is so great that it is not at first apparent how to utilize the data for improving sea ice data sets and models. A solution to this conundrum is offered in the RADARSAT Geophysical Processor System (RGPS), which takes 400 ScanSAR images every 24-day cycle and produces gridded products of ice motion, deformation and thickness. These geophysical products can be put to a variety of uses: analyzing new ice climatologies, testing ice models or new ideas about sea ice rheology, and for assimilating into sea ice models.

For the first time, we can produce basin-scale estimates of sea ice age and thickness from observations of ice motion in SAR images of the Arctic Ocean. The thickness distribution of sea ice is an essential descriptor of its mass and heat balance. Currently, we have only crude estimates on how much ice there is, how it varies in space and time, where ice is produced and where it melts, and how rapidly it is transported from place to place. Our present knowledge of the Arctic ice thickness distribution is derived largely from analyses of sonar data from submarine cruises. Moored upward looking sonars have also been used to sample the thickness distribution at fixed locations. However, these observations do not provide a complete spatial picture or continual updates of the thickness distribution. The new analysis technique described here allows us to monitor the spatial and temporal variability of the thin ice distribution (< 2m) in the Arctic Ocean using high-resolution SAR imagery.

This new method estimates ice age and thickness from repeated observations of Lagrangian elements or cells of sea ice in sequential SAR imagery. Fig. 1 shows the time series of observations of one cell within a matrix of such cells, graphs of the history of cell area, and the thin ice coverage within that cell at the end of a 41-day period. Line segments connecting the four vertices of a cell define its boundaries. The drift and deformation of a cell over time are obtained by tracking the displacement of its vertices in the SAR imagery. The motion tracking procedure is described in *Kwok et al.* (1995).

The age histogram of the ice in a cell is computed from the temporal record of area changes. An age histogram of sea ice specifies the fractional area covered by ice of different chronological ages. To construct this histogram from sequential observations, we follow the steps below. Every time a new observation is available, we interpret a positive area change as the creation of an area of open water. New ice is assumed to grow over this area immediately after opening. The uncertainty of the ice age occupying this area is dependent on the time interval between observations. This age range is recorded as a new age category in the histogram. At the same time a new category is introduced, existing age categories are 'aged' by the same time interval. In Fig. 1, this procedure created five ice age categories from the sequence of positive area changes since Day 335. A negative change is assumed to have ridged the youngest ice in the cell, reducing its area. The assumption here is that once ridging starts, the deformation tends to be localized in the recently-formed thinner and weaker ice in leads. This area of ridged ice is tracked as a separate category in the age histogram.

Ice age is converted to ice thickness using an empirical ice growth formula. We approximate the growth rate as a function of the number of freezing-degree days (FDD) associated with each age category using Lebedev's parameterization (discussed in *Maykut*, 1986) with $H = 1.33\ F^{0.58}$, where H is thickness and F is the accumulated freezing-degree days of that category. Volume is conserved when ice is ridged. We assume that all ridged ice is five times its original thickness and occupies a quarter of the area [*Parmerter and Coon*, 1972].

We start this scheme at fall freeze-up by covering the entire Arctic Ocean with initial 10 km by 10 km square elements, except near the ice margins where 25 km by 25 km are used. Complete coverage of the Arctic takes approximately 70,000 cells. At start up, the ice age/thickness histograms within the cells are unknown. In the process described, the ice volume created over a season is recorded in the thin ice thickness distribution and the ridge volumes. Since we do not melt ice in our scheme, the procedures above work only during the winter ice growth season. The results provide fine age/thickness resolution of only the young/thin end of the age/thickness distributions, but this is the crucial range that produces the most ice growth, the most turbulent heat flux to the atmosphere and the most salt flux to the ocean.

The backscatter intensity of each SAR sample is used to provide an independent estimate of the multiyear (MY) fraction within each cell. The MY algorithm [*Kwok et al.*, 1995] uses a maximum likelihood classifier and a look-up table of expected backscatter characteristics to assign an image pixel to one of two classes: multiyear ice and first-year ice. We assume that the area of MY ice fraction within a cell remains constant throughout the winter (by definition, no multiyear ice is created). Any anomaly in the classification process due to the backscatter variability of other ice types would show up as transients or spikes. These anomalies are filtered out in the time series of MY fraction estimates in each cell.

Two Examples

Over an ice growth season, the area occupied by each cell acquires a temporal description of the following properties: location, ice age and thickness histograms, deformation, and backscatter histogram. We select two of these properties to illustrate the large-scale character of the ice cover as revealed by 37,000 cells covering an area of approximately 4 x 10^6 km^2. Fig. 2 shows the temporal and spatial variability of cell divergence over three 14-day periods in 1996. Between November 10 and November 23, the high concentration of convergent cells in the eastern Beaufort Sea above 75N adjacent to the Canadian Archipelago and Greenland coast indicate extensive pressure ridging of the ice cover. In contrast, the eastern Arctic toward Siberia has a more divergent character. Due to the

convergence, the sampled ice cover lost approximately 3.5% of the area over this period. The next period, November 24 through December 7, shows very distinctive diamond-shaped lead patterns over the ice cover. Except for the regions near the ice margin, all the deformation is localized along leads while the rest of the ice cover remains unaffected. The length of some of the leads are quite remarkable, several leads can be seen to span a large fraction of the Arctic Ocean. The entire ice cover, except for the openings along the margin of the Beaufort Sea, stayed fairly quiescent with minimal lead activity during the last period from December 8 - 21. The area of the sampled ice cover increased by 2% and 1% during these two periods.

Fig. 3 shows the coverage of three categories of thin ice on December 21, at the end of the third periods. Approximately 3%, 5% and 1% of the area is covered by sea ice between 0-30 cm, 30-60 cm and 60-90 cm in thickness. The spatial distribution of the thinnest ice category is a record of the most recent divergence in the ice cover. It is highly correlated with the divergence field in Fig. 2c. Only lead ice that has not ridged in convergent events can survive to grow into the thicker ice. There is a distinct absence of thicker (60-90 cm) sea ice in the western Arctic probably due to the extensive convergence of the ice cover during the first period. On December 21 1996, approximately 3.5% of the area is covered by ridged ice formed during the 41 days.

The RGPS Program

These procedures described above are implemented in the RGPS – a data processing system dedicated to the analysis of large volumes of SAR imagery of sea ice required by the above process [*Kwok*, 1998]. The objective of RGPS is to produce Arctic-wide fields of ice motion and estimates of ice age and thickness from sequential SAR imagery for a series of winters.

The source of SAR imagery is the Canadian RADARSAT imaging radar. The radar was launched in November of 1995 into a 24-day repeat cycle, an orbit configuration that provides near repeat coverage of the high latitudes at 3- and 7-day intervals. This C-band radar has an imaging mode that illuminates a wide swath (460 km) and is well-suited for

large-scale mapping of the Earth surface. To support the data needs of the RGPS, we have been using this mode to acquire repeat coverage of the Arctic Ocean at near 3-day intervals since November of 1996. Over a 24-day repeat cycle of the satellite, we have close to eight observations of the western Arctic Ocean within the Alaska SAR Facility Reception mask. The repeat coverage of the Eurasian Basin is less frequent (6-days) due to the additional cost of RADARSAT data down-linked at the Tromso Satellite Station in Norway. We expect to continue this acquisition process over the life of the RADARSAT mission. The input SAR imagery is processed to a spatial resolution of approximately 100 m by 100 m, and is calibrated and archived at ASF.

The RGPS produces the following data products: Lagrangian ice drift; ice age histograms and thickness histograms; backscatter histograms; ice deformation; and the dates of melt onset and freeze up. These products contain ice motion of the vertices of the cells as well as the ice age/thickness histograms of each cell. The distribution of backscatter within each cell is stored as histograms. Ice deformation is the divergence, shear and vorticity of a cell derived from velocity gradients computed from ice motion at the cell vertices. The dates of spring melt and fall freeze are detected by changes in the backscatter record of each cell [*Winebrenner* et al., 1998]

More than two years of almost continuous observations of the Arctic Ocean have been acquired with RADARSAT. We started processing the RADARSAT imagery into sea ice products in January, 1999. The current throughput is approximately 1 cycle of RADARSAT data (over 400 frames) every 30 days. The intention is to eventually process all the RADARSAT data of the Arctic Ocean in the ASF archive. The RGPS Science Working Group addresses issues on product and algorithm development, and product validation.

Data Availability

At the time of this writing, we have processed more than 2-cycles (48-days) of RADARSAT data acquired between November and December of 1996. Later this year, our effective throughput will increase to one cycle every 15 days with the addition of a

new system. We expect to complete the processing of the 1996/97 winter data in December of 1999. Processing of the winter 1997/98 data will begin in June of 1999. Currently, the data products, documentation and software for reading the products are available on the web: http://www-radar.jpl.nasa.gov/rgps. The web site also contains animation of sequences of deformation fields. Later this year as more RGPS products are generated, they will become available through the EOS Data Gateway as well as the above web site.

References

Kwok, R., D. A. Rothrock, H. L. Stern and G. F. Cunningham, Determination of Ice Age using Lagrangian Observations of Ice Motion, *IEEE Trans. Geosci. Remote Sens.*, Vol. 33(2), 392-400, 1995.

Kwok, R. The RADARSAT Geophysical Processor System, in *Analysis of SAR data of the Polar Oceans: Recent Advances*, Tsatsoulis, C. and R. Kwok, Eds., Springer-Verlag, 235-258 ,1998.

Maykut, G. A., The Surface Heat and Mass Balance, in *Geophysics of Sea Ice*, Ed. N. Untersteiner, 395 –463, Series B: Physics Vol. 146, Plenum Press, 1986.

Parmerter, R. R. and M. Coon, Model of pressure ridge formation in sea ice, *J. Geophys. Res.*, 77, 6565-6575, 1972.

Winebrenner, D. P., D. G. Long and B. Holt, Mapping the progression of melt onset and freeze-up on Arctic sea ice using SAR and scatterometry, in *Analysis of SAR data of the Polar Oceans: Recent Advances*, Tsatsoulis, C. and R. Kwok, Eds., Springer-Verlag, 129-144,1998.

Figure Captions

Figure 1. Time series observations of one Lagrangian element in RADARSAT imagery. a) The deformation of a cell over a period of 41 days. The area of the cell stays fairly constant until Day 338 when a lead opens. The same lead continued to open between Days 341 and 345 contributing new ice area and ice categories to the cell. At the end of the 41-day period, the area of the thin ice occupies more that 50% of the total cell area; b) The history of the area of the cell; c) The thin ice categories occupying the new areas created since day 312. The largest thin ice category was created between days 341 and 345.

Figure 2. Cell divergence over three 14-day periods in the winter of 1996. a) November 10 through November 23; b) November 24 through December 7; c) December 8 through December 21. Red indicates divergence while blue indicates convergence.

Figure 3. Thin ice coverage on December 21, 1996. a) 0 – 30 cm; b) 30 – 60 cm; c) 60 - 90 cm. The colors indicate the fraction of each cell covered by thin ice in that thickness range. For example in Figure 3a, red indicates 10% of the cell is covered by ice of thickness 0-30 cm.

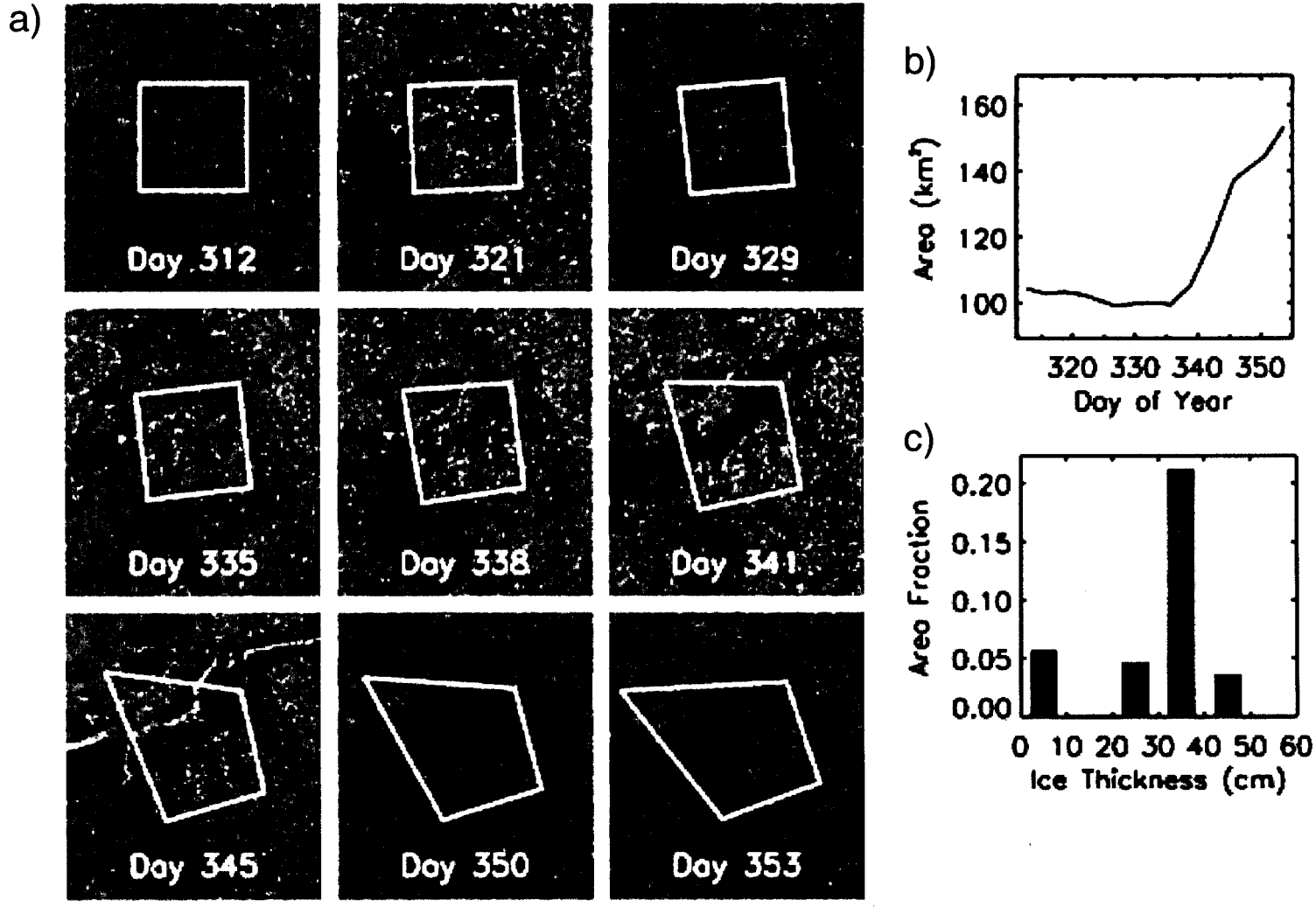
a)
Day 312
Day 321
Day 329
Day 335
Day 338
Day 341
Day 345
Day 350
Day 353
b)
Area (km²)
160
140
120
100
320 330 340 350
Day of Year
c)
Area Fraction
0.20
0.15
0.10
0.05
0.00
0 10 20 30 40 50 60
Ice Thickness (cm)

Fig. 1

a. Nov 10 - Nov 23

b. Nov 24 - Dec 7

c. Dec 8 - Dec 21

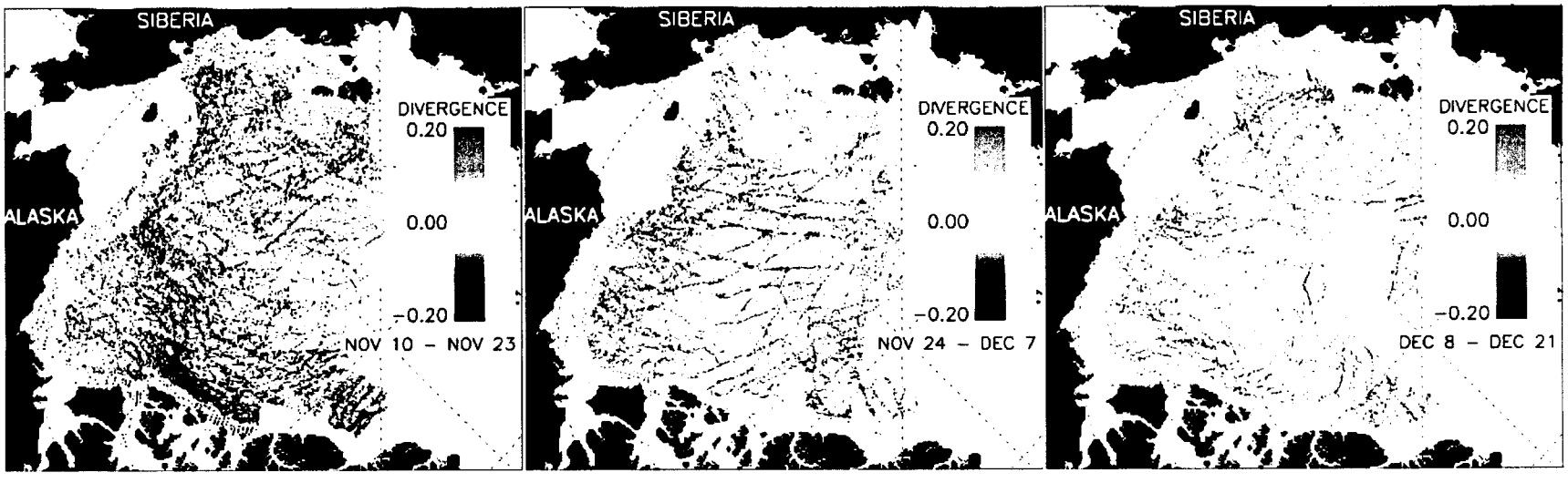

Fig. 2

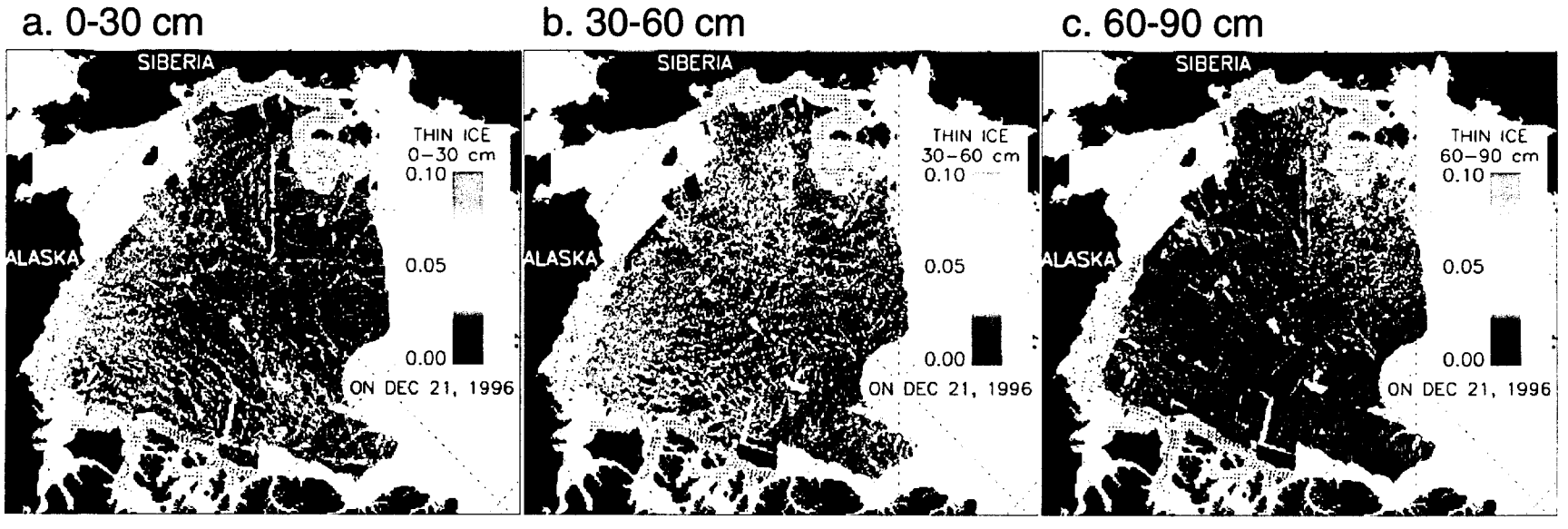
a. 0-30 cm
b. 30-60 cm
c. 60-90 cm
SIBERIA
ALASKA
THIN ICE
0–30 cm
30–60 cm
60–90 cm
0.10
0.05
0.00
ON DEC 21, 1996

Fig. 3